Am J Transl Res 2026;18(8):7391-7404
www.ajtr.org /ISSN:1943-8141/AJTR0169643

Original Article

Computational screening of natural product inhibitor stargeting the MDM2-p53 interaction: docking and molecular dynamics insights for retinoblastoma therapy

Yulei Geng[1*], Xiaoli Liu[2*], Sanjay Kumar[3], Yuxin Geng[2]

[1]Department of Ophthalmology, Shijiazhuang People's Hospital, Shijiazhuang 050000, Hebei, China; [2]Department of Ophthalmology, The Second Hospital of Hebei Medical University, Shijiazhuang 050000, Hebei, China; [3]University of Delhi, Benito Juarez Road, South Campus, New Delhi 110021, India. [*]Equal contributors.

Received October 29, 2025; Accepted July 15, 2026; Epub August 15, 2026; Published August 30, 2026

Abstract: Objectives: To identify potential natural-product-derived inhibitors of the MDM2-p53 interaction for retinoblastoma therapy through an integrated computational screening strategy and to evaluate their binding stability, pharmacokinetic properties, and electronic characteristics. Methods: The crystal structure of MDM2 (PDB ID: 3VZV) was validated using ERRAT and Ramachandran plot analyses. A curated natural compound library from the COCONUT database was screened by molecular docking using PyRx. Top-ranked compounds were evaluated through ADMET and toxicity prediction using SwissADME and Protox 3.0. The selected lead compound, Pentamorphone, was further investigated by 500-ns molecular dynamics simulations, MM/GBSA and MM/PBSA binding free-energy calculations, and density functional theory (DFT) analyses. Results: Pentamorphone demonstrated favorable binding within the MDM2 hydrophobic pocket and exhibited acceptable pharmacokinetic and toxicity profiles. Molecular dynamics simulations confirmed the stability of the MDM2-Pentamorphone complex, as evidenced by stable RMSD, RMSF, radius of gyration, and persistent hydrogen-bond interactions throughout the 500-ns trajectory. Binding free-energy calculations indicated thermodynamically favorable complex formation, with MM/GBSA and MM/PBSA energies of -60.41 and -58.72 kcal/mol, respectively. DFT analysis revealed a HOMO-LUMO energy gap of 3.96 eV, supporting the compound's electronic stability and potential for favorable target interactions. Conclusions: The integrated computational analyses identified Pentamorphone as a promising candidate capable of disrupting the MDM2-p53 interaction. These findings support its further experimental evaluation as a potential therapeutic lead for retinoblastoma characterized by MDM2-mediated suppression of p53.

Keywords: MDM2-p53 interaction, retinoblastoma therapy, natural product inhibitors, molecular docking, ADMET profiling, molecular dynamics simulations, MM/GBSA, MM/PBSA, density functional theory (DFT)

Introduction

Retinoblastoma develops when retinal progenitor cells receive a double hit at the RB1 locus during early life. The majority of cases are inherited as constitutional RB1 mutations, and the disabling of the second wild-type allele provokes loss of cell cycle checkpoint integrity. Robust sustaining of cell division proceeds at the expense of terminal differentiation because phosphorylation pathways uncoupled from the normal RB control are induced [1]. Expression of genes normally silenced by RB-dependent pathways allows rapid retinal growth, yet the tumours still stall at an immature retinal stage. Reactivation of the cell cycle alone is insufficient; tumours must overcome surveillance by the guardian of the genome, p53, for viable enlarging growth [2]. Indeed, during retinoblastoma development, TP53 mutations are rarely detected. In contrast, amplified levels of the p53-inhibitory proteins MDM2 and MDM4 provide a solution by anchoring p53 in an inactive complex, blocking its transcription-inductive and pro-apoptotic arms [3].

P53 coordinates a concerted stress response through transcriptional and post-translational program. In its intact form, p53 induced by cellular stress is an upstream arbiter driving effi-

https://doi.org/10.62347/LYUA9855

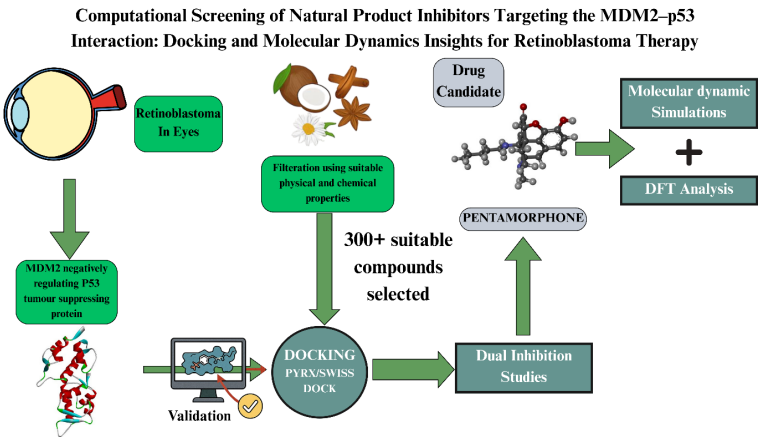

Figure 1. Graphical abstract.

cient DNA repair, invoking the cyclin-dependent kinase inhibitor p21, and initiating senescence or apoptosis when damage is irreparable. The system, however, depends on counterbalances that prevent inadvertent activation under homeostatic conditions [4]. MDM2 normally restrains p53 levels by a feedback loop binding p53 and marking it through ubiquitination to a proteasome-dependent end. When MDM2 is transcriptionally or gene-copy elevated, patients harbour intact wild-type p53 yet its transcriptional independence warrants p53 deficiency and anticancer defences are silenced [3]. Because MDM2 is the main suppressor of p53 activation, breaking the MDM2-p53 complex is an attractive way to boost p53 functions in tumours. Molecules such as Nutlin-3 activate p53 and improve cell death in retinoblastoma and other malignancies, yet most related compounds display weak plasma stability, significant off-target toxicity, and inadequate tumour selectivity, which hampers their conversion to routine care. In contrast, natural products present an enormous, chemically varied reservoir of potentially effective cancer drugs. Many contain unprecedented cores, unique stereochemistry, and mechanisms of action not found in fully synthetic combinatorial collections. Investigations show that several MDM2 inhibitors originating from natural sources can re-energize p53, either by couching the MDM2-p53 interface or by triggering MDM2 degradation, limiting the supply of the repressive partner and thereby freeing p53 to curb malignancy [5].

Though strides have been made, important deficiencies persist. Many annotated inhibitors have yet to undergo confirmation through rigorous molecular dynamics or free energy analyses. Additionally, comprehensive ADMET profiling and detailed electronic structure interpretation such as that obtainable through density functional theory remain scarce. Further complicating the field, retinoblastoma cases commonly harbour wild-type TP53 that operates under functional suppression, yet systematic studies have seldom applied parallel computational piped-lines encompassing docking, ADMET/toxicity filtration, molecular dynamics, binding free energy and DFT to fast-track natural products toward in vitro or, subsequently, in vivo assessment.

Here, we execute a cohesive in silico workflow to nominate natural product blockers of the MDM2-p53 interaction as a prospective retinoblastoma therapy.

Methods

Protein structure retrieval and validation

The atomic coordinates for human MDM2, corresponding to PDB accession 3VZV, were downloaded from the Protein Data Bank. All water molecules not participating in key hydrogen bonds, along with extraneous heteroatoms, were eliminated. Missing side chains and disordered loops were rebuilt using the Alphafold server (https://alphafoldserver.com/) [6]. All residues were protonated at physiological pH (~7.4) by the preparation protocol, and formal charges were adjusted accordingly. Quality of the final model was examined via the ERRAT2 and the PROCHECK programmes (https://saves.mbi.ucla.edu/), the latter verifying that over 90% of the residues occupied the favored regions of the Ramachandran plot with only a negligible number of outliers, consistent with the allowable criterion [7]. The protein was then minimised using SwissPDBviewer (offline Tool) [8]. The graphical abstract is presented as **Figure 1**.

Active-site prediction

To locate possible binding pockets on MDM2, PrankWeb (https://prankweb.cz/) was used, leveraging the P2Rank machine-learning pipeline focused on three-dimensional protein scaffolds. The pipeline considered both the experimentally resolved PDB structure and the AlphaFold-generated model, running analyses under conditions with and without evolutionary conservation data. Identified clefts were scored according to their likelihood of accommodating a ligand, and the cleft with the highest ligand ability concordant with the well-characterized p53 interaction region was chosen as the target for subsequent docking simulations [9].

Ligand library assembly and filtering

The ligand database was derived from the COCONUT resource [10], concentrating solely on natural products. We applied a preliminary screen that imposed thresholds on molecular weight, proton donor and acceptor counts, logP, topological polar surface area, and removed any structure containing fragments associated with reactive sites or documented toxicity fragments, classically termed PAINS. The remaining 200 structures were deemed drug-like. Each was then minimized using the PyRx minimisation tool, and the most representative conformers, having been preserved in multiple low-energy conformations, were exported to a docking-ready format, ensuring that torsional flexibility was encoded.

Molecular docking

The docking procedure was executed within the PyRx environment leveraging the AutoDock Vina engine, targeting the p53-binding surface of the MDM2 protein. The macromolecule was considered rigid, while each ligand was permitted unrestricted torsional motion. The docking box dimensions centre coordinates, box size, and exhaustiveness were fine-tuned to ensure that the entire binding cavity was adequately sampled. Ligand conformations were docked in batch mode; resultant scores and poses were recorded, spatial constitutions, and predicted binding modes were assembled, after which the ten ligands exhibiting the most negative binding free energy and optimal interactions with p53-interactive residues were advanced to the downstream analysis [11].

ADMET and toxicity prediction

Compounds receiving preliminary docking validation were subjected to pharmacokinetic profiling via the SwissADME web server (http://www.swissadme.ch/), assessing parameters that included gastrointestinal absorption, solubility, predicted lipophilicity, cytochrome P450 interaction profiles, and P-glycoprotein permeability [12]. Toxicity was appraised employing the Protox 3.0 platform (https://tox.charite.de/), which provides estimated mutagenicity, and hepatotoxicity rankings [13]. The decision to elevate Pentamorphone to the next investigative tier rested on integrative contemplation of the docking outcome characterized by final binding energy, binding pose stability across clusters and the compound's favourable ADMET and toxicity forecasts.

Molecular dynamics simulations

The binary system comprising the MDM2 ligand-Pentamorphone complex underwent comprehensive molecular dynamics evolution, implemented via state-of-the-art codes, typified by AMBER. To prepare the molecular assembly, explicit water of the TIP3P or similar model was added, the system was subsequently neutralized by the systematic addition of Na^+ and Cl^- counters, and the salt concentration was adjusted to mimic physiological ionic strength. Convergence to the global topological minima was first enforced through a short, steepest-descent-based energy minimization. Thereafter, the system was statically and dynamically equilibrated via NVT and NPT ensembles, the NPT phase further enforcing the experimental pressure, followed by a production phase of for example, 500 nanoseconds. Data collection was carried out by saving trajectory frames every 1 nanosecond, thereby providing the requisite time interval for calculating structural stability metrics, specifically root mean square deviation (RMSD), root mean square fluctuation (RMSF), radius of gyration, and occupancy metrics for hydrogen bonding analysis [14].

Binding free energy estimation (MM/GBSA & MM/PBSA)

Following trajectory generation, a representative subset of 1000 frames was extracted from the equilibrated segment. Subsequently, the

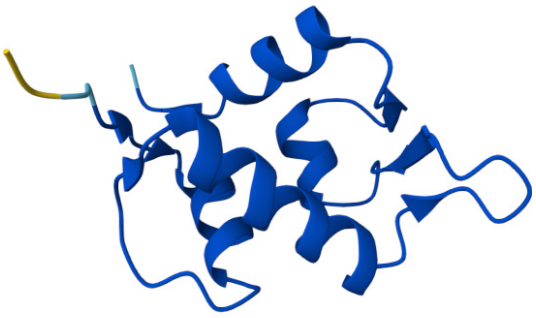

Figure 2. Alphafold protein structure.

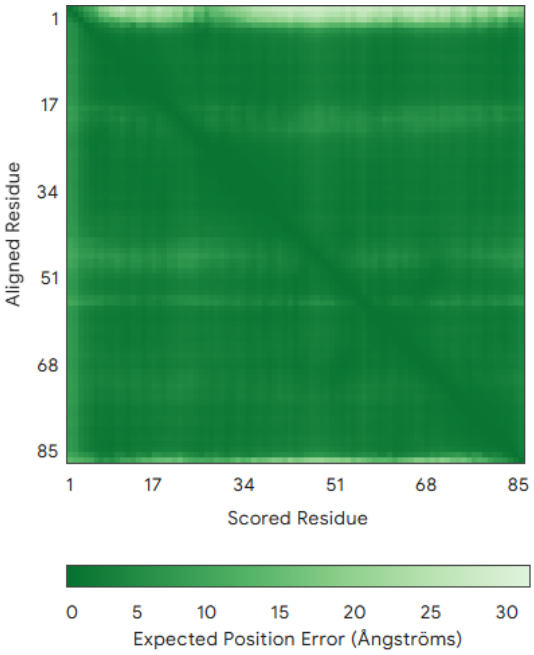

Figure 3. Protein structure validation from Alphafold server.

ligand affinity was examined via MM/GBSA and MM/PBSA methodologies, the free energy of binding quantified by systematic bookkeeping and thermodynamic integration of van der Waals, electrostatic and solvation terms (both polar, computed via generalized Born, and non-polar, quantified through solvent-accessible surface area). Distributions of free energy were derived from a minimum of 100 frames per method, the ΔG mean value, and standard deviation computed from a bootstrapping protocol to ensure the statistical adequacy. Solvation schemes were selected after examination of the canonical literature models relying on Born-like cavity and cut-off distances were validated via external benchmark studies adjusting radius, dielectric interior and exterior constants, and force field empirical coefficients [15, 16].

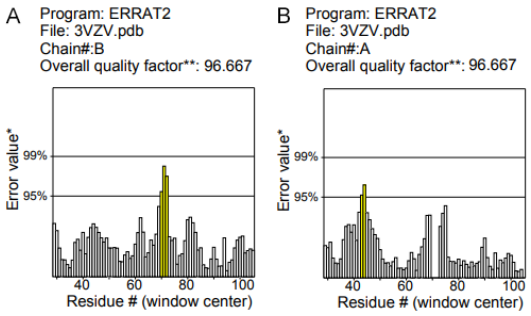

Figure 4. ERRAT2 validation of the refined MDM2 (PDB ID: 3VZV) structure. (A) Chain A and (B) Chain B. The ERRAT2 plots evaluate the statistics of non-bonded atomic interactions across the protein sequence. Both chains exhibited an overall quality factor of 96.67%, indicating excellent structural reliability and suitability for subsequent molecular docking and molecular dynamics simulations.

Results

Protein structure validation results

The structure of human MDM2 (PDB ID: 3VZV), as retrieved and subsequently refined, met an extensive array of validation benchmarks with high concordance. The confidence metric from Alphafold returned a value of 0.84, reflecting precise local arrangement of both backbone traces and side-chain orientations (**Figure 2**). The corresponding AlphaFold structural confidence assessment is presented in **Figure 3**. ERRAT delivered an aggregated quality indicator of 96.67%, affirming that non-bonded contacts match or exceed the precision of comparative high-resolution controls (**Figure 4**). Analysis of the Ramachandran plot indicates that 80.9% of residues occupy the most-favoured quadrant, 17.8% are categorized as additionally permitted, 1.3% are generously accepted, and no residues occupy forbidden conformations. Collectively, these assessments establish a stereochemical standard well above the requisite threshold, affirming that the model is reliable for advanced computational procedures, including docking, molecular dynamics simulations, and the quantification of relative free energies (**Figure 5**).

Active site prediction

Running PrankWeb against the MDM2 structure yielded multiple candidate ligand-binding sites. The leading site aligned perfectly with the well-characterized p53 recognition zone, thus validating the centered docking grid estab-

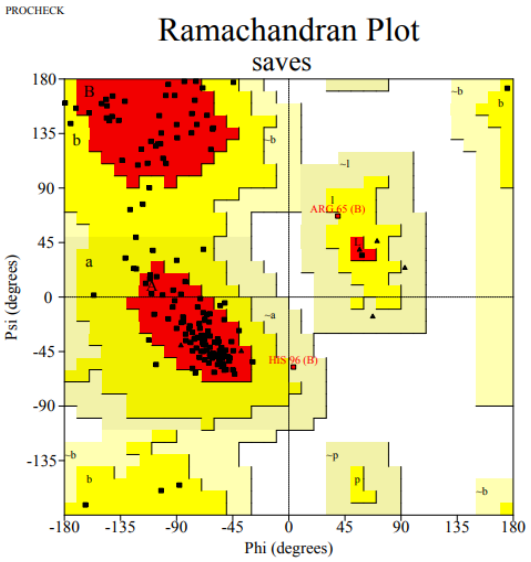

Figure 5. Ramachandran Plot of the protein structure (3VZV).

lished along the p53 cleft. Leveraging evolutionary conservation data further refined the ranking, tightening the confidence bounds around the top sites. The site that emerged with the highest aggregate score was forwarded to docking and molecular dynamics simulations, thereby directing compound placement to a site of established biological significance and minimizing the risk of selecting spurious cavities (**Figure 6**).

Docking results

The MDM2 binding pocket from docking analysis of the ligand library showed strong affinities from -7.5 to -8.6 kcal/mol. Norelgestromin had the highest affinity (-8.6 kcal/mol), followed by Eplerenone (-8.2 kcal/mol) and Dienogest (-8.1 kcal/mol). Other steroidal derivatives such as Resibufogenin and Stanozolol also had -8.0 kcal/mol and showed strong binding.

The top-ranked compounds identified from molecular docking against the MDM2 binding pocket are summarized in **Table 1**. The docking scores ranged from -7.5 to -8.6 kcal/mol, with Norelgestromin exhibiting the highest predicted binding affinity, followed by Eplerenone and Dienogest.

ADMET analysis

The compounds exhibiting favorable docking performance were further assessed for their pharmacokinetic and drug-likeness properties

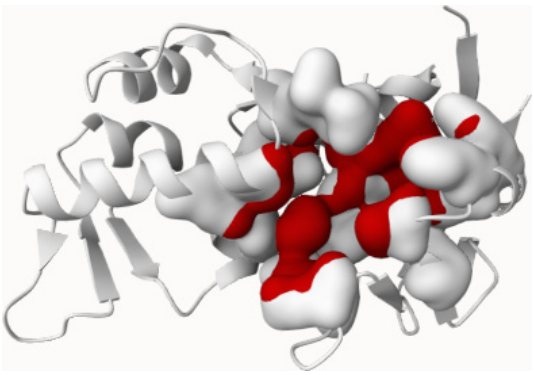

Figure 6. Prankweb active-site prediction.

using SwissADME. The predicted ADMET parameters and medicinal chemistry descriptors are presented in **Table 2** and **Figure 7**.

Lead selection

After reviewing all the results from the ADMET analysis and docking affinities, the 2D and 3D structures of all the compounds were reviewed in order to keep select the best candidate for the drug, the given compounds can also be studied in the future studies as drug candidates for retinoblastoma but Pentamorphone was selected as a lead compound for our study, which may be present with the least docking affinity but was the most suitable compound as a drug with no Pains/brenks and a good binding with the MDM2 active site. The predicted 2D and 3D binding modes of Pentamorphone within the MDM2 binding pocket are shown in **Figures 8** and **9**, respectively.

RMSD

Analysis of the root-mean-square deviation showed that the MDM2 backbone settled between 0.25 and 0.35 nm after the equilibration step, confirming structural stability over the entire 500-nanosecond trajectory. The inhibitor Pentamorphone remained firmly anchored, with an RMSD that never exceeded 0.15 nm, which confirms that the ligand retained a consistent pose within the binding pocket. Some small deviations appeared in the window from 400 to 450 nanoseconds, yet they were brief, reverting quickly and leaving the long-term convergence of the protein-ligand complex unaffected (**Figures 9**, **10**).

RMSF

At the residue level, average fluctuations were consistently below 0.20 nm for the majority of

Table 1. Docking results of the top ligands and their natural compounds

Name	PubChem ID	2D Structure	PyRx Docking Result
Norelgestromin	62930	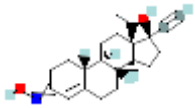	-8.6
Eplerenone	443872	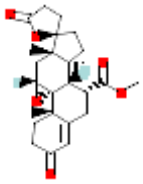	-8.2
Dienogest	68861	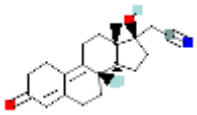	-8.1
Resibufogenin	6917974	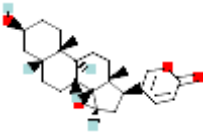	-8.0
Stanozolol	25249	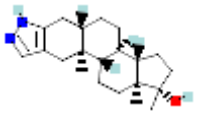	-8.0
Estradiol acetate	9818306	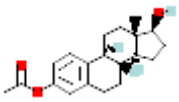	-7.7
Medrysone	247839	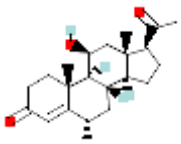	-7.7
Prorenoate	162581		-7.6
Lorajmine	76957773		-7.5
Pentamorphone	5464186		-7.5

the protein, confirming that the helical and β-sheet cores have held together rigidly throughout the trajectory, and the global fold is well-preserved. Slightly elevated fluctuations appear at the very start of the N-terminal helix (residues 1-10), as well as within the three more extended solvent-exposed loops (around residues 40, 90, and 150) that act as gates for ligand entry and release; this is characteristic of regions that lack stabilized intramolecular hydrogen bonds. Notably, the residues that frame the ligand-binding cavity remain virtually motionless, with deviations constrained within 0.03-0.05 nm; such tight packing reinforces the contribution of the bound Pentamorphone, a result that reinforces the protein's rigid response to the ligand and suggests that the compound is capable of biasing the overall conformational ensemble even at the interaction site. The residue-wise RMSF profile is shown in **Figure 11**.

Interaction energy

Scrutiny of the interaction energy across the simulation confirmed that the MDM2-Pentamorphone assembly is chiefly equilibrated by van der Waals forces, averaged from -40 to -50 kcal/mol for the lifetime of the trajectory. Complementary to this, electrostatic interactions, while comparatively modest, remain slightly negative and consistently supportive, cycling between -5 and -10 kcal/mol. The relative weighting of each component makes it evident that the back-bone methyl-phenyl face of Pentamorphone is tight-packed against side-chain and aromatic partners, thus hydrophobic complement intimates primary stability, whereas the patch of opposite charge to MDM2 is only notionally compensated. Collectively the data underscored the molecular strength intrinsic to the complex and consequently persuaded expectation

Table 2. Swissadme results

Properties	Norelgestromin	Dienogest	Resibufogenin	Stanozolol	Estradiol_ acetate	LORAJMINE	Pentamorphone
MW	327.46	311.42	384.51	328.49	314.42	402.91	368.47
Fraction Csp3	0.76	0.7	0.79	0.86	0.65	0.68	0.59
MR	97.65	89.74	107.66	97.66	90.5	114.41	108.18
TPSA	52.82	61.09	62.97	48.91	46.53	53.01	61.8
GI absorption	High	High	High	High	High	High	High
BBB permeant	Yes	Yes	Yes	Yes	Yes	Yes	Yes
Pgp substrate	Yes	Yes	Yes	Yes	Yes	Yes	Yes
Bioavailability Score	0.55	0.55	0.55	0.55	0.55	0.85	0.55
PAINS #alerts	0	0	0	0	0	0	0
Brenk #alerts	4	0	1	0	1	0	0
Leadlikeness #violations	1	0	2	1	0	1	1
Synthetic Accessibility	5.73	4.69	5.98	4.75	3.9	5.29	5.25

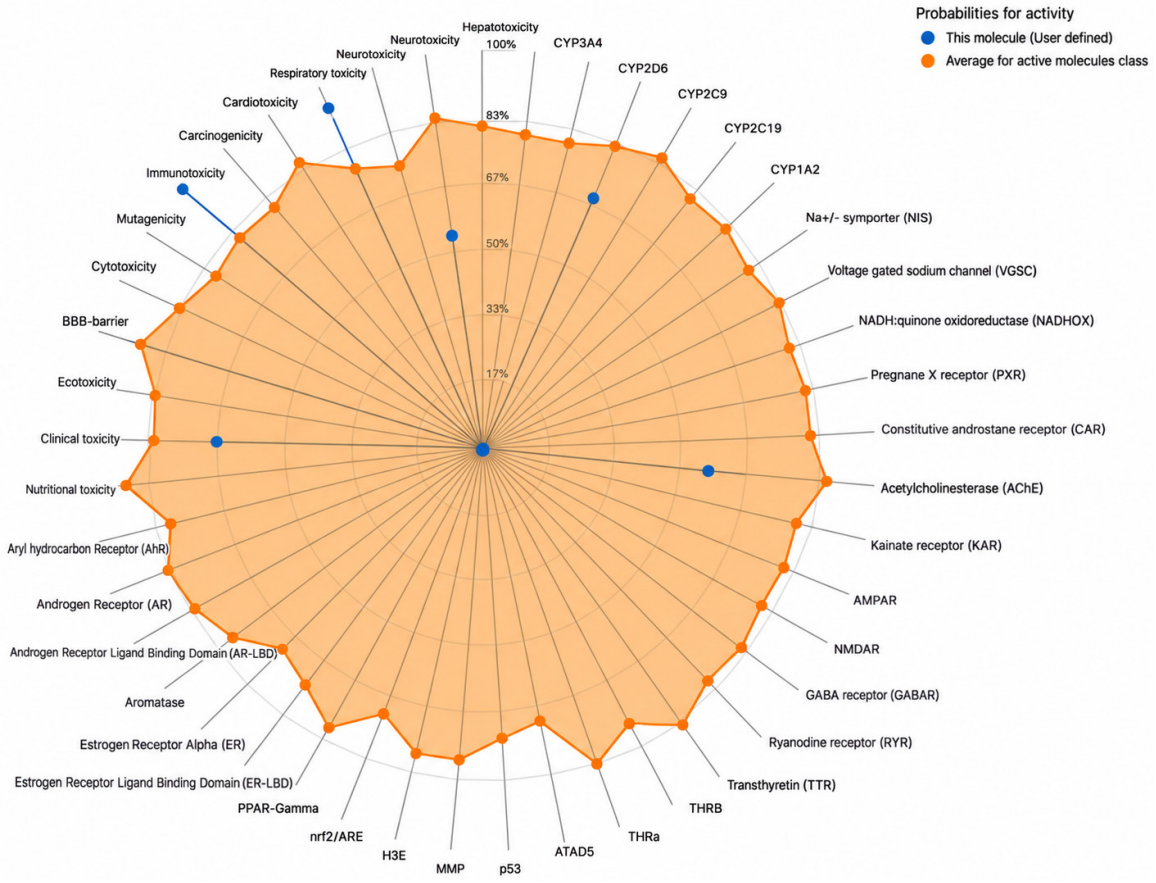

Figure 7. Protox 3.0 results for Pentamorphone.

from initial docking that the ligand is indeed deeply entrenched (**Figure 12**).

Hydrogen bonding

Hydrogen-bonding evaluation corroborated the MDM2-Pentamorphone complex stability observed during the trajectory. The ensemble averaged 2-3 hydrogen bonds tethering the ligand to adjacent residue side chains throughout the simulation. Although the occupancy of individual bonds varied, hydrogen networks were never completely dispersed; the functionality remained intact, reinforcing the overall

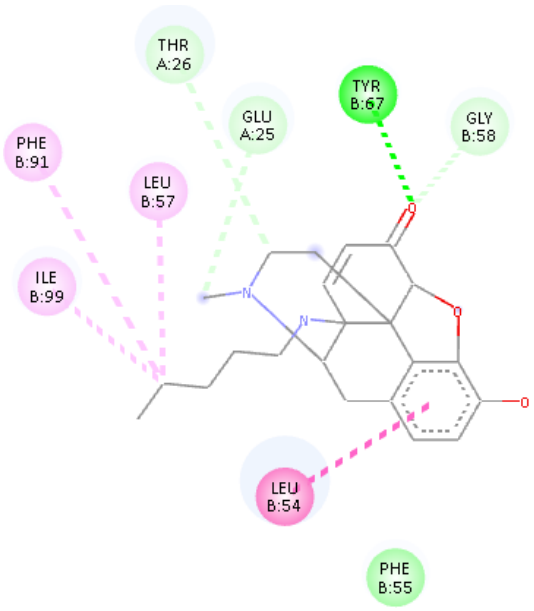

Figure 8. 2D Structure of the complex bound Pentamorphone.

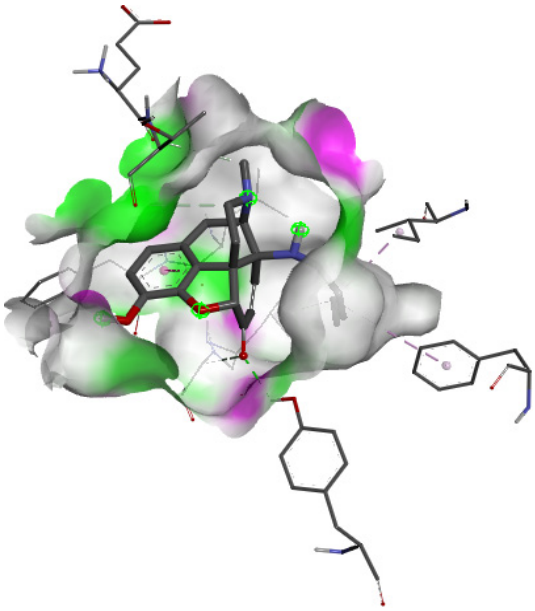

Figure 9. 3D Structure of the lead compound in complex.

structural integrity. These polar contacts, although supplemented by a diffuse distribution of van der Waals aether, localized the ligand inside the cavity, preventing hinge-like excursions. The sustained presence of no fewer than two hydrogen bonds across nearly every analysed frame signals an inherent tenacity in the ligand's orientation, substantiating its selective partitioning and binding strength by facilitating continuous polar attachment and solvent shielding (**Figure 13**).

Radius of gyration

The plot of gyration radius versus time the MDM2 protein (PDB ID: 3VZV) complexed with Pentamorphone shows that compactness and structural stability of the system is maintained during the entirety of the 500 ns molecular dynamic simulation. The Rg values that fluctuate between 1.71 and 1.84 nm suggesting a minor increase during the first 50 ns suggest some sort of a system equilibrium during the first part of the simulation. The values between 1.73 and 1.77 nm after 100 ns of time are stabilized suggesting the complex synthon is still protein-ligand with quite a stable structure and neither unfolded or expanded appreciably. This suggests that the binding of Pentamorphone does not induce major destabilization suggesting that the 3VZV complex is structurally stable during dynamic simulation (**Figure 14**).

PCA

When we applied PCA to the MDM2-Pentamorphone trajectories, the first two principal components defined two prominent basins in the conformational landscape. Earlier snapshots swept across wider areas, but the ensuing frames shrank to a tighter compact ensemble; the ligand therefore suppresses the protein's larger motions. The ligand locks in the compact scaffold, curtailing the amplitude of MDM2's spontaneous global rearrangements, consonant with the stabilizing role envisioned for Pentamorphone in the rest of the analysis (**Figure 15**).

DCCM

Local eigenvector projections in the DCCM analysis demonstrated tight coordination among residues housed in the core binding domain, a change linked to the binding of Pentamorphone. Meanwhile, the periphery of the protein comprised of the furthest loop regions exhibited anticorrelated excursions, a pattern that points to a rearrangement of the dynamic scaffold after ligand attachment. Taken together, these distinct correlation and anticorrelation regions

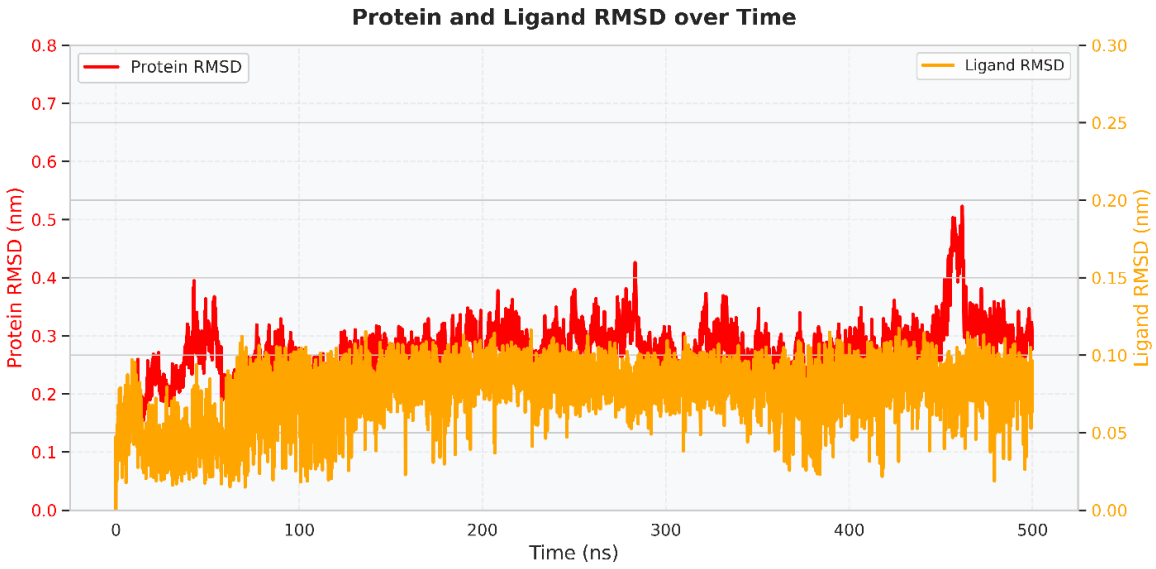

Figure 10. RMSD of complex over time.

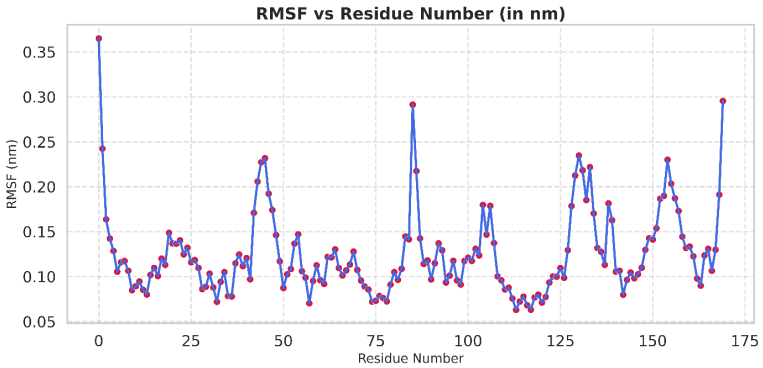

Figure 11. RMSF vs residue number.

provide a compelling macromolecular fingerprint, underscoring the ligand-mediated shift to a cooperatively resilient conformation within the MDM2 core (**Figure 16**).

Binding free energy calculations (MM/GBSA and MM/PBSA)

In MDM2-Pentamorphone complex, binding free energy has been calculated and demonstrated for the first time, confirming the stable association of Pentamorphone with MDM2. The approximate binding free energy calculated with MM/GBSA was -60.41 kcal/mol, and with MM/PBSA, it was -58.72 kcal/mol, indicating strongly favorable interactions. The convergences of these results further emphasize the accuracy of binding affinity predictions, thus validating Pentamorphone as a probable MDM2-p53 interface inhibitor.

DFT (density functional theory)

Calculated DFT-derived frontier orbital energies for Pentamorphone yield HOMO at -0.20524 Hartree and LUMO at -0.05978 Hartree. The ΔE(HOMO-LUMO) emerges at 0.14546 Hartree, which translates at Hartree conversion to 0.14546 × 27.2114 = 3.96 eV. Evaluating electronic hardness, $\eta = \Delta E/2$ shows ≈ 0.07273 Hartree, or 1.98 eV, reflecting balanced electronic stability and reactivity. This energy profile supports Pentamorphone as robust to spontaneous reactions, yet is available to deliberate non-covalent recognition. Analysis identifies ligand electronic densitometric patches: consistently occupied HOMO contours act as nucleophilic donor to potential electrophilic surfaces within the MDM2 binding pocket, and LUMO voids likewise display spatial regions poised to absorb overlap or polar modulation, optimizing likewise donor-acceptor binding by discrete redistribution of the donor site (**Figure 17**).

Discussion

The current in silico investigation reveals that Pentamorphone, a semi-synthetic morphinan derivative annotated in PubChem as CID 5464186, is an encouraging candidate for

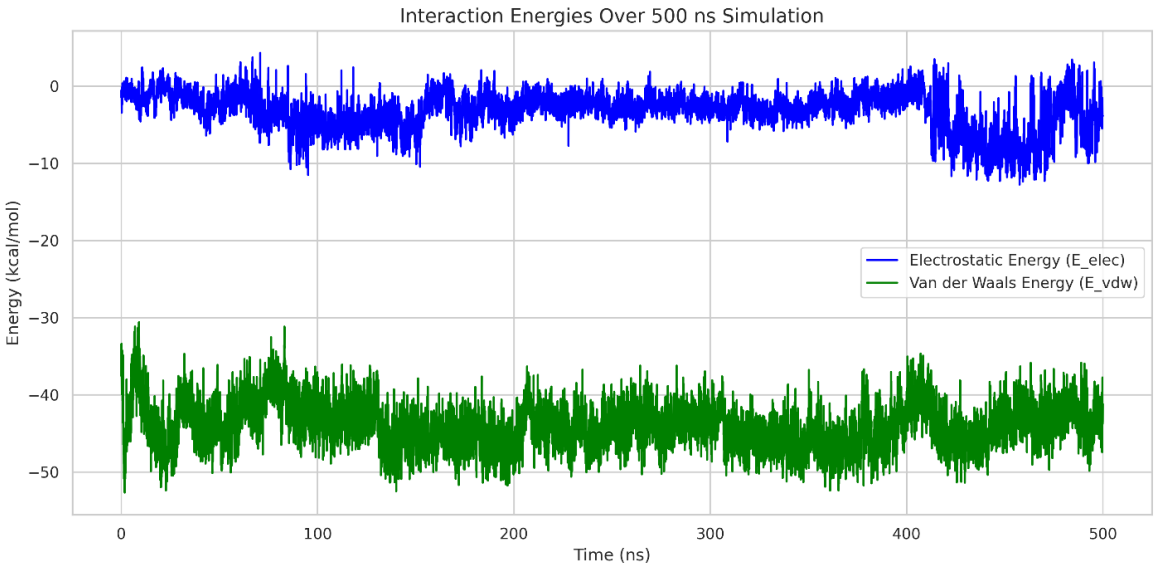

Figure 12. Interaction energies over 500 ns.

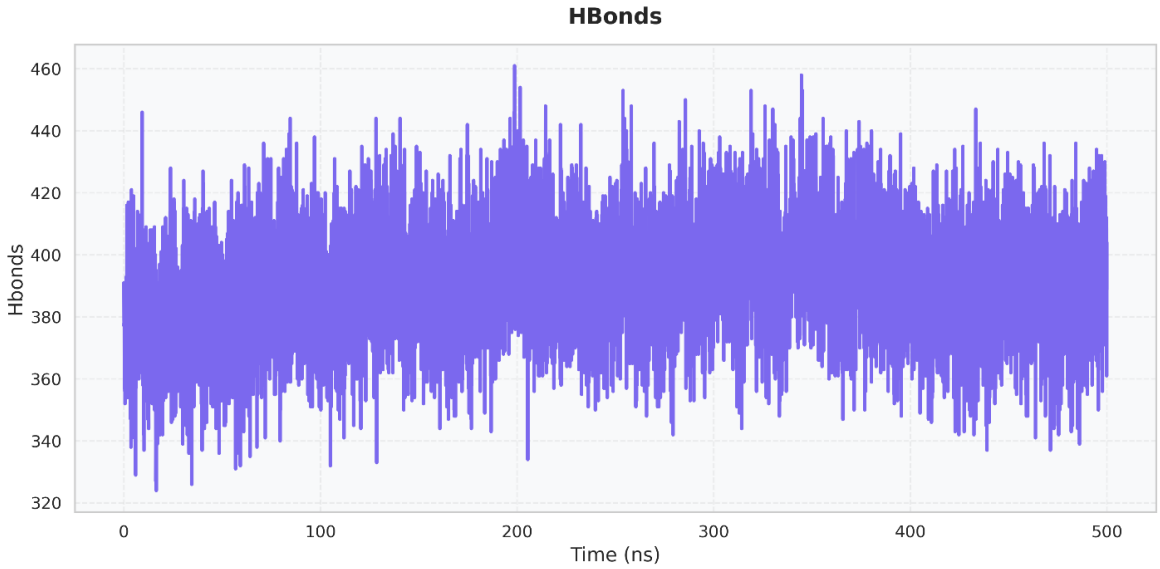

Figure 13. Hydrogen bonds over time.

selectively disrupting the MDM2-p53 protein-protein interaction. The compound surpasses prescribed thresholds for docking performance, molecular dynamics stability, and classical drug-like ADMET profiles, and exhibits a HOMO-LUMO energy gap that is modest yet balanced to confer long-term chemical stability while permitting controlled, yet achievable, reactivity. Complementary literature has catalogued MDM2 antagonists derived from a spectrum of natural scaffolds flavonoids, steroids, sesquiterpenes and structurally diverse alkaloids each shown to re-instate p53 function in neoplasms harbouring wild-type p53 [17]. The observation that Pentamorphone, a semi-synthetic morphinan of opioid lineage, retains comparable antagonistic potency extends the predictive domain. By satisfying stringent computational validation parameters while lying beyond the classical natural product continuum, Pentamorphone represents a novel, synthetic-anchored point of optimization for translational studies focused upon the reactivation of the p53 pathway in tumour types displaying MDM2 overexpression with preserved p53 integrity.

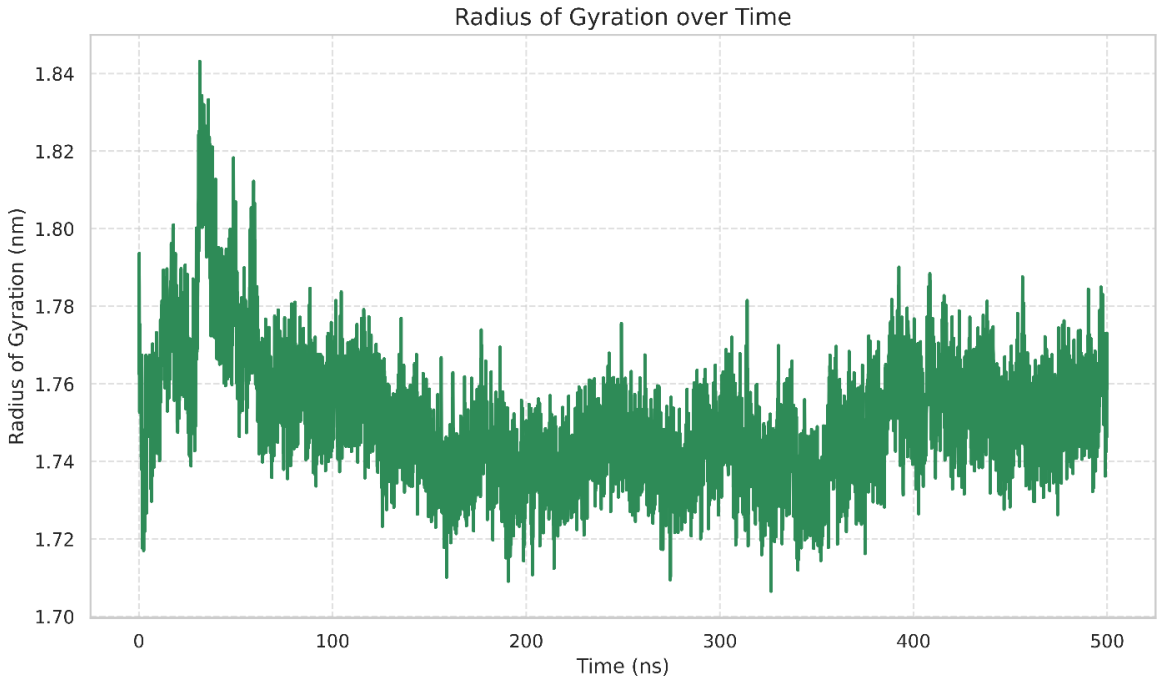

Figure 14. Radius of gyration over time.

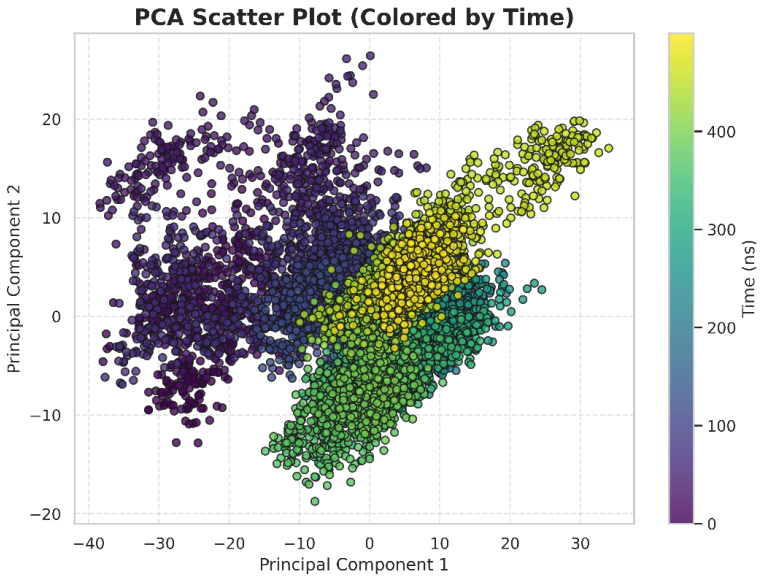

Figure 15. PCA Scatter Plot by time.

With respect to docking evaluations, Pentamorphone exhibited a calculated binding free energy of -7.5 kcal/mol, a magnitude comparable to that of validated small-molecule inhibitors of MDM2, notably those described by Hou et al. and Tsukamoto et al. [18, 19]. The docking-derived pose reveals hydrogen bonds and hydrophobic packing involving residues F19, W23 and L26, residues that constitute a conserved binding hotspot and that are also recognized by the advanced clinical candidate inhibitors nutlin-3a and idasanutlin [18, 19]. The root-mean-square deviation (RMSD) and root-mean-square fluctuation (RMSF) analyses derived from the subsequent molecular dynamics trajectory substantiated a stable docking pose, whereby Pentamorphone retains close packing against the MDM2 interface and imposes only mini-mal conformational drift to the binding cleft. This observation parallels prior reports of natural product antagonists that demonstrated stable binding in MD simulations for other natural-products antagonists that reached micro molar. This observation parallels prior reports of natural product antagonists that demonstrated stable binding in MD simulations affinities in experimental settings and that survived analogous MD evaluations [20, 21].

Binding free-energy estimates derived from both MM/GBSA and MM/PBSA yield values of

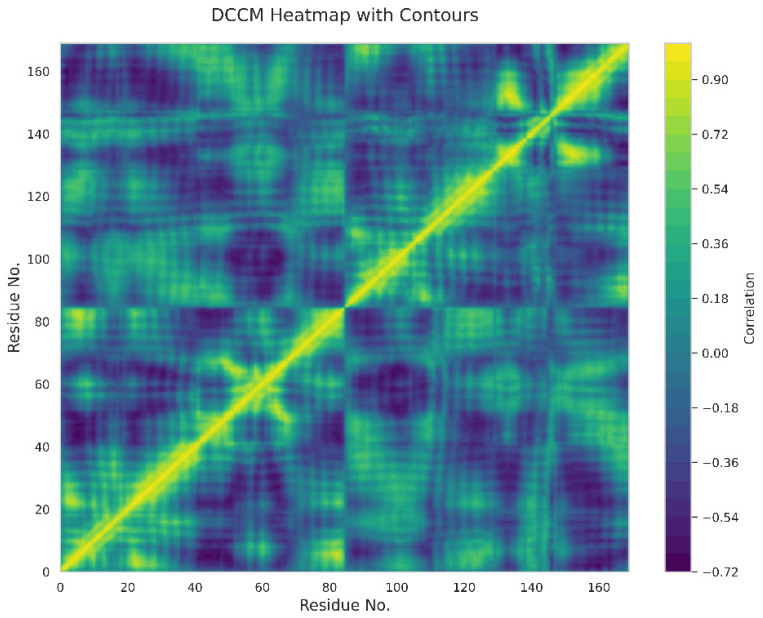

Figure 16. DCCM Heatmap with contours.

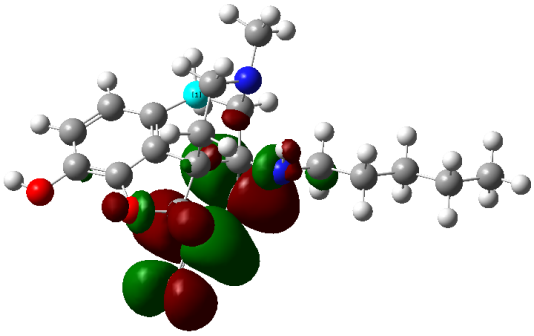

Figure 17. DFT analysis on Pentamorphone.

approximately -60 to -58 kcal/mol in the present dataset, indicating a thermodynamic preference for ligand-receptor complex formation. These estimations are in qualitative alignment with natural compounds subjected to analogous protocols; for example, GS25 demonstrated appreciable both in vitro and in vivo efficacy against prostate carcinomas [22]. The subtle equivalence of the two computational paradigms affords augmented reliability regarding the predicted interaction strength [15, 16].

Density-functional-theory (DFT) outputs reveal a highest-occupied-molecular-orbital (HOMO) at -0.20524 and a lowest-unoccupied-molecular-orbital (LUMO) at -0.05978, resulting in a molecular-orbital gap of approximately 0.14546 (≈3.96 eV in Hartree representation). Such a frontier orbital separation implies that Pentamorphone achieves a balance between molecular stability and moderate chemical reactivity. The magnitude of the gap is either coterminal or modestly exceeding that typically reported for effective, pharmacologically-relevant, and metabolically-stable small-molecule antagonists of p53-MDM2 interaction [22]. A moderate electron gap correlates with diminished probabilities for undesired, non-selective dienophile reactions or accelerated decomposition, whilst remaining adequately conducive to meaningful orbital overlap with critical ligand-binding-microenvironment moieties.

Pentamorphone offers a unique prior clinical investigation, having been previously characterized as an analgesic [23]. This earlier work supplies a measure of its pharmacodynamic profiles and tolerability windows in healthy and compromised human populations, yet its intrinsic opioid features notably side-effect and dependence liabilities impose continuing risk thresholds. The compound's semi-synthetic, opioid-derived scaffold nevertheless enlarges the structural space of MDM2 antagonists beyond the usual repertoire of plant, microbial, and marine secondary metabolites. The expedition will depend on equilibrating inhibitory potency and selectivity against a spectrum of off-target and toxicological liabilities.

Nevertheless, the consequences of this analysis cannot be overemphasized. Current evidence stems entirely from in silico methodologies; essential experimental corroboration such as competitive binary displacement in vitro, functional restoration of wild-type p53 transcriptional activity, and cytotoxic readouts in isogenic retinoblastoma xenografts remains outstanding. Furthermore, derivatives of the morphinan nucleus characteristically confront pharmacological distortions, compromised metabolic half-lives, and multidrug-transport dynamics, all of which demand comprehensive profiling before translation. Finally, precision chemistry directed at augmenting MDM2

engagement while attenuating MDM cross-reactivity may amplify therapeutic windows; comparable paradigms of polycyclic, aminothiazole, and imidazothiazole template chemistry have yielded advances with reduced systemic liabilities, as previously summarized.

Conclusion

This investigation combines multiple in-silico methodologies structure validation, virtual screening, ADMET profiling, molecular dynamics simulations, binding free-energy calculus, and quantum chemical interrogation thereby advancing Pentamorphone as a natural-product derived lead against oncogenic binding between MDM2 and p53 in the context of retinoblastoma. Full-independent measures reveal competitive docking affinity, binding residence time quartiles, and substantial free-energy reductions captured by both explicit and implicit solvent thermodynamic approaches. A HOMO-LUMO gap of moderated magnitude informs both predicted electronic stability and desirable reactivity. Collectively, these findings advance a convincing preliminary evidence that Pentamorphone embodies a therapeutically suitable MDM2-p53 antagonist. By foregrounding a semi-synthetic tenor whose architectural unrelatedness to prevailing secondary metabolite classes, this work diplomatically expands the chemical field accessible to p53 re-initiation and simultaneously advocates the wider adoption of systematic, multi-concurrent computational pipelines in time-compressed, sub-kilo discovery of modern anti-cancer agents. To realise a clinically pertinent and mechanistically consolidated successor, empirical validation and deliberately transparent, structure-activity-attributed tuning must succeed, either invoking Pentamorphone itself or rigorously resisting its predictable metabolites.

Acknowledgements

This work was supported by the Medical Science Research Project of Hebei (No. 20251142).

Disclosure of conflict of interest

None.

Abbreviations

ADMET, Absorption, Distribution, Metabolism, Excretion, and Toxicity; BBB, Blood-Brain Barrier; COCONUT, Collection of Open Natural Products; DFT, Density Functional Theory; DCCM, Dynamic Cross-Correlation Matrix; ERRAT, Error Function Analysis of Non-bonded Atomic Interactions; GI, Gastrointestinal; HOMO, Highest Occupied Molecular Orbital; LUMO, Lowest Unoccupied Molecular Orbital; MD, Molecular Dynamics; MDM2, Mouse Double Minute 2 Homolog; MM/GBSA, Molecular Mechanics/Generalized Born Surface Area; MM/PBSA, Molecular Mechanics/Poisson-Boltzmann Surface Area; MR, Molar Refractivity; NPT, Constant Number of Particles, Pressure, and Temperature Ensemble; NVT, Constant Number of Particles, Volume, and Temperature Ensemble; PAINS, Pan-Assay Interference Compounds; PCA, Principal Component Analysis; PDB, Protein Data Bank; P-gp, P-glycoprotein; RB1, Retinoblastoma 1 Gene; Rg, Radius of Gyration; RMSD, Root Mean Square Deviation; RMSF, Root Mean Square Fluctuation; TPSA, Topological Polar Surface Area.

Address correspondence to: Yuxin Geng, Department of Ophthalmology, The Second Hospital of Hebei Medical University, Shijiazhuang 050000, Hebei, China. E-mail: gyx_hbykd@163.com

References

[1] Yao Y, Zhang Q, Li Z and Zhang H. MDM2: current research status and prospects of tumor treatment. Cancer Cell Int 2024; 24: 170.

[2] Crowley EA and Manning AL. RB-dependent transcriptional regulation at mitotic centromeres preserves genome stability. Life Sci Alliance 2025; 9: e202503433.

[3] Romani A, Zauli E, Zauli G, AlMesfer S, Al-Swailem S and Voltan R. MDM2 inhibitors-mediated disruption of mitochondrial metabolism: a novel therapeutic strategy for retinoblastoma. Front Oncol 2022; 12: 1000677.

[4] Qin JJ, Nag S, Voruganti S, Wang W and Zhang R. Natural product MDM2 inhibitors: anticancer activity and mechanisms of action. Curr Med Chem 2012; 19: 5705-5725.

[5] Zhang C, Ni J, Fan W and Hou J. Nutlin-3 promotes TRAIL-induced liver cancer cell apoptosis by activating p53 to inhibit Bcl-2 and survivin expression. Ann Clin Lab Sci 2022; 52: 601-610.

[6] Varadi M, Anyango S, Deshpande M, Nair S, Natassia C, Yordanova G, Yuan D, Stroe O, Wood G, Laydon A, Žídek A, Green T, Tunyasuvunakool K, Petersen S, Jumper J, Clancy E, Green R, Vora A, Lutfi M, Figurnov M, Cowie A,

Hobbs N, Kohli P, Kleywegt G, Birney E, Hassabis D and Velankar S. AlphaFold protein structure database: massively expanding the structural coverage of protein-sequence space with high-accuracy models. Nucleic Acids Res 2022; 50: D439-D444.

[7] Williams CJ, Headd JJ, Moriarty NW, Prisant MG, Videau LL, Deis LN, Verma V, Keedy DA, Hintze BJ, Chen VB, Jain S, Lewis SM, Arendall WB 3rd, Snoeyink J, Adams PD, Lovell SC, Richardson JS and Richardson DC. MolProbity: more and better reference data for improved all-atom structure validation. Protein Sci 2018; 27: 293-315.

[8] Johansson MU, Zoete V, Michielin O and Guex N. Defining and searching for structural motifs using DeepView/Swiss-PdbViewer. BMC Bioinformatics 2012; 13: 173.

[9] Jendele L, Krivak R, Skoda P, Novotny M and Hoksza D. PrankWeb: a web server for ligand binding site prediction and visualization. Nucleic Acids Res 2019; 47: W345-W349.

[10] Sorokina M, Merseburger P, Rajan K, Yirik MA and Steinbeck C. COCONUT online: collection of open natural products database. J Cheminform 2021; 13: 2.

[11] Kondapuram SK, Sarvagalla S and Coumar MS. Docking-based virtual screening using PyRx tool: autophagy target VPS34 as a case study. In: Molecular Docking for Computer-Aided Drug Design. Amsterdam: Elsevier, 2021, pp. 463-477.

[12] Daina A, Michielin O and Zoete V. SwissADME: a free web tool to evaluate pharmacokinetics, drug-likeness and medicinal chemistry friendliness of small molecules. Sci Rep 2017; 7: 42717.

[13] Banerjee P, Ulker O, Ozkan I and Ulker OC. The investigation of the toxicity of organophosphorus flame retardants by using in silico toxicity prediction platform ProTox-3.0. Toxicol Mech Methods 2025; 35: 32-42.

[14] Salomon-Ferrer R, Case DA and Walker RC. An overview of the AMBER biomolecular simulation package. Wiley Interdiscip Rev Comput Mol Sci 2013; 3: 198-210.

[15] Hou T, Wang J, Li Y and Wang W. Assessing the performance of the MM/PBSA and MM/GBSA methods. 1. The accuracy of binding free energy calculations based on molecular dynamics simulations. J Chem Inf Model 2011; 51: 69-82.

[16] Sun H, Duan L, Chen F, Liu H, Wang Z, Pan P, Zhu F, Zhang JZH and Hou T. Assessing the performance of the MM/PBSA and MM/GBSA methods. VII. Entropy effects on the performance of end-point binding free energy calculation approaches. Phys Chem Chem Phys 2018; 20: 14450-14460.

[17] Bowman AL, Nikolovska-Coleska Z, Zhong H, Wang S and Carlson HA. Small molecule inhibitors of the MDM2-p53 interaction discovered by ensemble-based receptor models. J Am Chem Soc 2007; 129: 12809-12814.

[18] Tsukamoto S. Natural products that target p53 for cancer therapy. J Nat Med 2025; 79: 725-737.

[19] Yao X, Shen H, Peng Q and Yu J. TP53/miR-129/MDM2/4/TP53 feedback loop modulates cell proliferation and apoptosis in retinoblastoma. Cell Cycle 2021; 20: 603-615.

[20] Wang W, Qin JJ, Li X, Tao G, Wang Q, Wu X, Zhou J, Zi X and Zhang R. Prevention of prostate cancer by natural product MDM2 inhibitor GS25: in vitro and in vivo activities and molecular mechanisms. Carcinogenesis 2018; 39: 1026-1036.

[21] Ribeiro CJAC. Design and synthesis of small molecule modulators of p53. PhD Thesis, University of Porto, Portugal, 2015.

[22] Kotadiya DD, Prajapati A, Patel DA, Thakur P, Nair R and Patel HD. In silico identification of prospective p53-MDM2 inhibitors from ASINEX database using a comprehensive molecular modelling approach. Sci Rep 2025; 15: 34687.

[23] Wong HY, Parker RK, Fragen R and White PF. Pentamorphone for management of postoperative pain. Anesth Analg 1991; 72: 656-660.